OMAE2015-42074

DEVELOPMENT OF PTO-SIM: A POWER PERFORMANCE MODULE FOR THE OPEN-SOURCE WAVE ENERGY CONVERTER CODE WEC-SIM

Ratanak So
Asher Simmons
Ted Brekken
School of Electrical Engineering and Computer Science
Oregon State University
Corvallis, Oregon USA

Kelley Ruehl [*]
Carlos Michelen
Water Power Department
Sandia National Laboratories
Albuquerque, NM USA
Email: kelley.ruehl@sandia.gov

ABSTRACT

WEC-Sim (Wave Energy Converter-SIMulator) is an open-source wave energy converter (WEC) code capable of simulating WECs of arbitrary device geometry subject to operational waves. The code is developed in MATLAB/Simulink using the multi-body dynamics solver SimMechanics, and relies on Boundary Element Method (BEM) codes to obtain hydrodynamic coefficients such as added mass, radiation damping, and wave excitation. WEC-Sim Version 1.0, released in Summer 2014, models WECs as a combination of rigid bodies, joints, linear power take-offs (PTOs), and mooring systems. This paper outlines the development of PTO-Sim (Power Take Off-SIMulator), the WEC-Sim module responsible for accurately modeling a WEC's conversion of mechanical power to electrical power through its PTO system. PTO-Sim consists of a Simulink library of PTO component blocks that can be linked together to model different PTO systems. Two different applications of PTO-Sim will be given in this paper: a hydraulic power take-off system model, and a direct drive power take-off system model.

INTRODUCTION

Sandia National Laboratories (SNL) and the National Renewable Energy Laboratory (NREL) have jointly developed WEC-Sim (Wave Energy Converter-SIMulator), an open-source

wave energy converter (WEC) design tool capable of running on a standard personal computer. WEC-Sim simulates WECs of arbitrary device geometry subject to operational waves [1]. The code is developed in MATLAB/Simulink using the multi-body dynamics solver SimMechanics, and relies on Boundary Element Method (BEM) codes to obtain hydrodynamic coefficients such as added mass, radiation damping, and wave excitation. The WEC-Sim hydrodynamic solution has been verified through code-to-code comparison, and has undergone preliminary validation through comparison to experimental data [2] [3] [4] [5]. Further validation of the WEC-Sim code will be performed upon completion of the WEC-Sim validation tank testing, planned for Summer 2015.

Version 1.0 of WEC-Sim, released in Summer 2014, models WECs as a combination of rigid bodies, joints, linear power take-offs (PTOs), and mooring systems. While the Version 1.0 release of the WEC-Sim code was limited to modeling PTOs as simple linear dampers, collaboration with the Energy Systems group at Oregon State University (OSU) has resulted in the development of PTO-Sim (Power Take Off-SIMulator). PTO-Sim is the WEC-Sim module responsible for accurately modeling a WEC's conversion of mechanical power to electrical power through its PTO system (or power conversion chain, PCC). It consists of a library of PTO component blocks that can be linked together to model different PTO systems. Each of these PTO library blocks is a model of common PTO components, such as electric gener-

---

[*]Address all correspondence to this author.

ators, pistons, and accumulators. Two different applications of PTO-Sim will be given in this paper: a hydraulic power take-off system model, and a linear direct drive power take-off system model.

POWER CONVERSION CHAINS

A WEC's power conversion chain converts the mechanical motion of the WEC into electrical power [6]. The majority of WECs convert the energy from the wave into either relative linear motion, relative rotary motion, or fluid capture. This mechanical power is then converted into electrical power through the WEC's PCC. There are many different possible PCC configurations, as shown in Fig 1. On the left side of the figure is the energy conversion mechanism, and on the right side are different PCC components with black arrows indicate possible PCC paths. The Color Legend refers to technological readiness level of each PCC component [7] [8]. This technological readiness level is based on the work in the DNV Recommended Practices which takes into consideration both the degree of the novelty of the technology and its intended application [9].

Based on a survey of the EERE WEC database, there are 34 WEC PCCs that are at a technology readiness level (TRL) 5 or greater [10]. Of these 34 WEC PCCs, 16 use a hydraulic PTO, 11 use a mechanical PTO, and 7 use a turbine, see Fig. 3. Of the 11 mechanical PTOs, 6 are direct drive systems. The results of this survey, and current trends in the WEC industry, drove the development of hydraulic and direct drive application cases PTO-Sim. These two application cases will be released with future versions of the WEC-Sim code. Since WEC-Sim is an open source code, and there are many different possible PCC configurations, users can create PCC specific models to meet their needs. These can be built based on existing PTO-Sim library blocks, or by creating new PCC component blocks.

PTO-SIM

WEC-Sim consists of a library of different WEC components, namely: bodies, joints and constraints. These WEC-Sim library blocks can be linked together to model the hydrodynamic behavior of different WEC devices. An example of applying the WEC-Sim code that used PTO-Sim to model the Reference Model 3 (RM3) point absorber is shown Fig. 2. The RM3 was designed as part of the DOE-funded Reference Model Project [11]. RM3 is a simple two-body heaving point absorber, consisting of a float and a damping plate. The float is connected to the damping plate through a translational joint which is actuated by the external PTO-Sim subsystem that simulates the PTO system. The damping plate is then connected to the seabed through a heave joint that constrains motion relative to the sea floor. This paper specifically focuses on what is inside the PTO-Sim block on the left side of Fig. 2.

PTO-Sim is developed in a similar manner to WEC-Sim, as a library of different PCC components. The PTO-Sim library has been developed based on the possible PCC configurations outlined in Fig 1. In the following sections, the PTO-Sim component library will be used to model a hydraulic PTO, and a direct drive PTO. WEC PCCs are complex and device specific, meaning that while some PTO models can be built directly from the PTO-Sim library, others will require custom PCC library components. For the purpose of describing the coupling between PTO-Sim and WEC-Sim, refer to Fig. 2, where the WEC-Sim relative displacement and velocity outputs (zRel and zDotRel respectively) are the PTO-Sim inputs. Similarly the PTO force (Fpto) is the WEC-Sim input, and the PTO-Sim output for both PTO architectures demonstrated in this paper. These signals are what couple WEC-Sim and PTO-Sim together. In order to demonstrate the functionality of PTO-Sim, the results presented in the following sections use a relative velocity (zDotRel) from WEC-Sim to run the PTO-Sim simulations, but the PTO-Sim force (Fpto) was not fed back into the WEC-Sim code (one-way coupling). A fully two-way coupling of PTO-Sim with WEC-Sim is under development.

Hydraulic PTO

An example of a hydraulic PTO used in a point absorber is shown in Fig. 4. The piston position and velocity are the relative displacement and velocity between the float and the spar. The first PTO system element is a double acting hydraulic piston pump, "P". This component directly converts the heave motion of the buoy into a pressurized, bi-directional fluid flow. The piston chamber is connected to a rectifying valve via terminals "A" and "B". This changes the bi-directional flow into a uni-directional flow and passes the fluid on to the rest of the system. The valves "1" through "4" indicate the different flow paths that perform this conversion. Valve "1" delivers fluid to the high pressure side of the system where it is stored in the high pressure accumulator "C". A variable displacement motor, "M", translates the hydraulic fluid power into rotational energy. The axle of the motor is connected directly (no gearboxes) to a generator axle ("G") , causing it to spin and generate electricity. The hydraulic motor was chosen to meet the torque and speed requirements. The hydraulic fluid then enters the low pressure side where accumulator "D" provides pressure control. The piston draws fluid from "D", completing the circuit [12].

The hydraulic PTO model begins with the continuity equation for a compressible fluid, which is used to describe the pressures in the piston chamber [13]:

$$\dot{p}_A = \frac{\beta_e}{V_o - A_p z}(A_p \dot{z} - \dot{V}_1 + \dot{V}_4) \qquad (1)$$
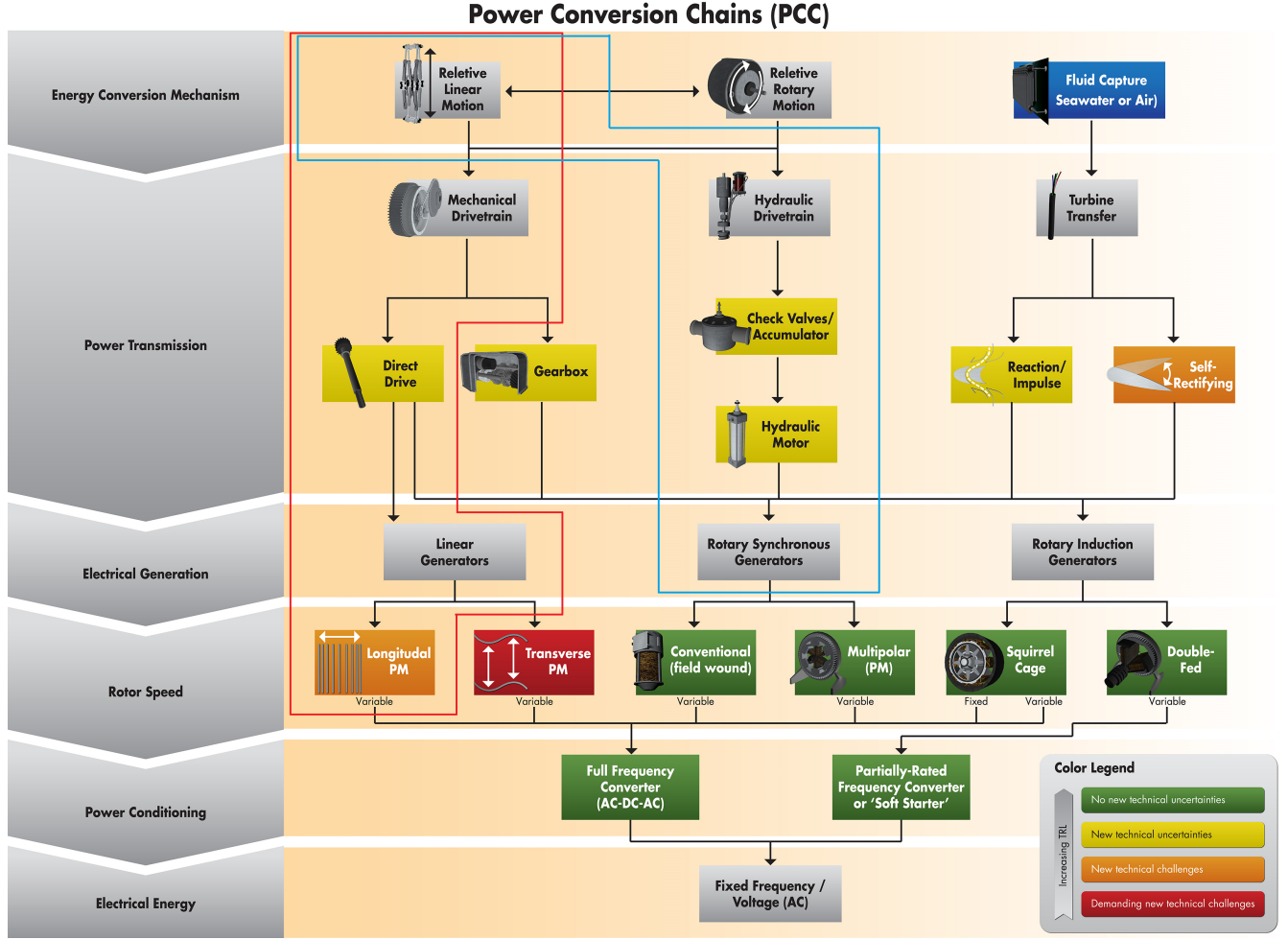
FIGURE 1. Power conversion chain from mechanical energy to electrical connection to grid. Lower TRLs are novel concepts and higher TRLs are more proven technology. The direct drive PTO path is shown in the red box outline and the hydraulic PTO path is shown in the blue box outline.

$$\dot{p}_B = \frac{\beta_e}{V_o + A_p z}(-A_p \dot{z} - \dot{V}_2 + \dot{V}_3) \qquad (2)$$

The effective bulk modulus of the hydraulic fluid is β_e, V_o is the initial volume of the cylinder, and A_p is the piston area. The volumetric flow through valves 1-4 are represented by $\dot{V}_1$ through $\dot{V}_4$. The piston and buoy are rigidly connected, and their movement with respect to the spar is the input to the PTO system. The relative motion between the buoy and the spar is represented by the velocity, $\dot{z}$ (from WEC-Sim).

The four valves in the rectifying circuit are each modeled using the orifice equation:

$$\dot{V}_i = C_d A_v \sqrt{\frac{2}{\rho}(p_j - p_k)\tanh(k_1(p_j - p_k))} \qquad (3)$$

The subscript "i" refers to the valve number. C_d is the discharge coefficient and A_v is the cross-section area of the orifice. Finally, p_j and p_k are the pressures on either side of the valve. The *tanh* function, being differentiable, enables certain control/optimization strategies as well as simplifying the calculations. Also, the *tanh* function multiplied by the pressure difference provides an analytic approximation to the absolute value function, where $k_1 \gg 0$. The valve area is modeled as a variable area poppet valve, with the equation:

$$A_v = A_{min} + \frac{A_{max} - A_{min}}{2} + \frac{A_{max} - A_{min}}{2}(\tanh(k_2(p_j - p_k - \frac{p_{max} + p_{min}}{2}))) \qquad (4)$$

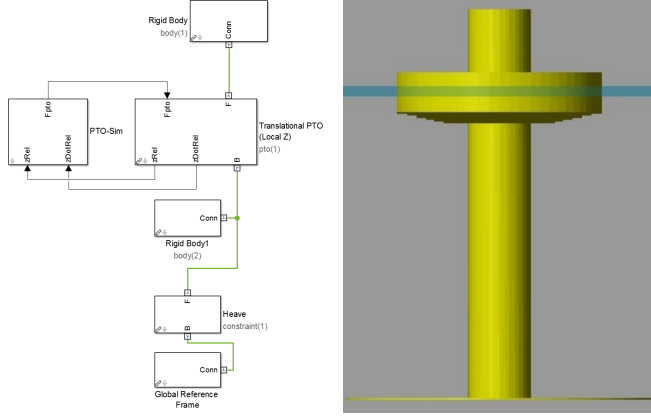where A_{max} and A_{min} are the maximum and minimum valve areas.

3

FIGURE 2. RM3 model with PTO-Sim (left) with the animation (right) [1].
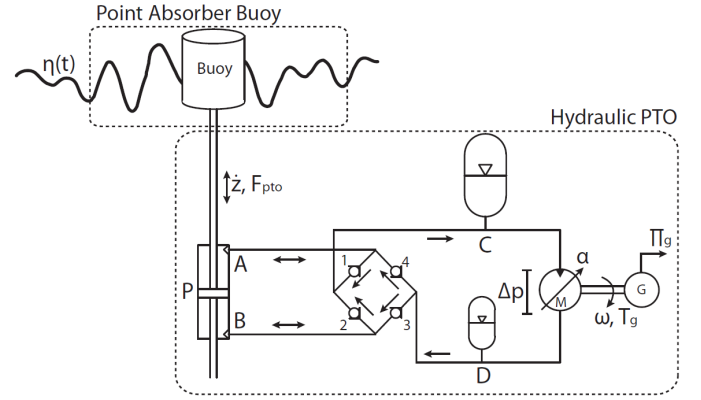

FIGURE 4. Schematic of the PTO-Sim hydraulic model. The arrow indicate the direction of flow.
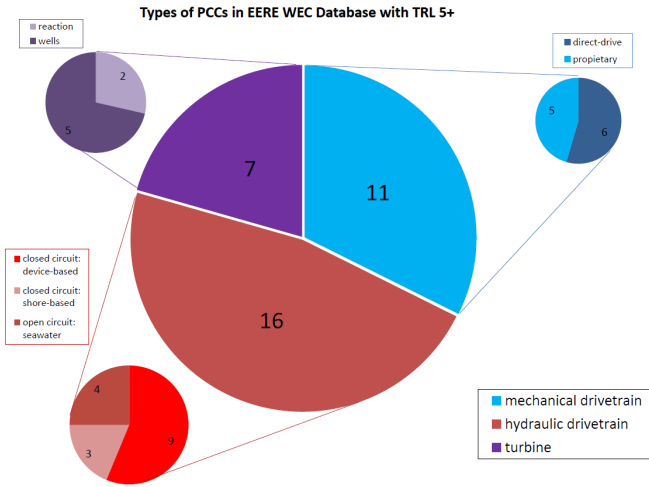

FIGURE 3. Breakdown of PCC types currently used by companies with TRL equal to or greater than 5.

FIGURE 5. Valve opening behavior as a function of pressure difference across the valve.

The valve begins to open when p_{min} is reached. The maximum pressure, p_{max} is the pressure for which the valve is fully opened. The *tanh* function in this equation provides a smooth approximation to the step operation of the valve. This is accomplished by choosing k_2 such that when the pressure difference (p_j - p_k) is equal to p_{max}, the valve area difference (A_v-A_{min}) is equal to A_{min}. The behavior of the valve is shown in Fig. 5.

The flow into the accumulators "C" and "D" are, respectively:

$$\dot{V}_C = -\alpha D\omega + \dot{V}_1 + \dot{V}_2 \qquad (5)$$

$$\dot{V}_D = \alpha D\omega - \dot{V}_3 - \dot{V}_4 \qquad (6)$$

where α is the swashplate angle ratio, which is the instantaneous motor displacement divided by the the maximum motor displacement. It is used as a control for the volumetric flow across the motor. D is the nominal motor displacement, and ω is the rotational speed of the generator. For this hydraulic system the swashplate angle ratio is fixed for the simulated sea state.

The pressure in each accumulator is dependent on the instantaneous volume of hydraulic fluid in the accumulator:
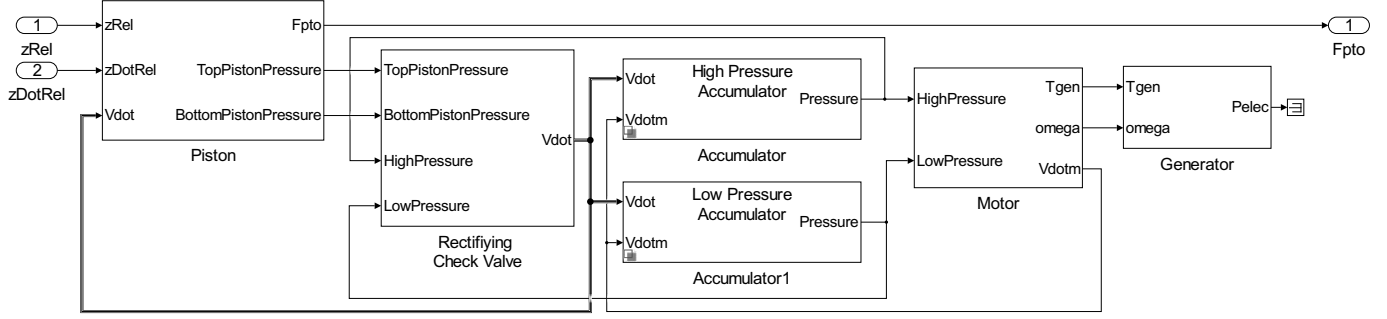
FIGURE 6. Simulink model of the hydraulic system.

$$p_i = \frac{p_{i0}}{(1 - \frac{V_i}{V_{i0}})^{1.4}} \quad (7)$$

where p_{i0} is the precharge pressure and V_{i0} is the total volume of the accumulator.

Because the motor axle and generator axle are rigidly connected, they have the same torque and opposite rotational direction. This condition leads to the state equation:

$$\dot{\omega} = \frac{1}{J_t}(\alpha D(p_C - p_D) - b_g\omega - b_f\omega) \quad (8)$$

The generator torque is represented by $b_g\omega$, the frictional damping is $b_f\omega$, and J_t is the total mass moment of inertia of the motor/generator drive train. The frictional damping was chosen to give the generator a 95% efficiency at a speed of 2400 rpm.

Finally, the PTO force is described by the A-B pressure differential and the piston area under pressure, A_p:

$$F_{pto} = (p_A - p_B)A_p \quad (9)$$

These equations are contained in PTO-Sim library blocks, representing physical components of the hydraulic PTO system. The complete hydraulic PTO model as implemented using PTO-Sim is shown in Fig. 6.

Simulations. Figures 7 and 8 show a sample (from 200-300 seconds) of the simulation. Figure 7 shows the system inputs, zRel (relative heave displacement) and zDotRel (relative heave velocity). Figure 8 shows the power produced by the PTO. The blue line, P_{abs} is the power absorbed at the piston. P_{mech}, the power at the axle connecting the motor and generator, is shown

in red. Finally, P_{elec} is the electrical power at the output of the generator, is shown in red. The generator model is based on the characteristics of a typical large industrial induction generator. The speed, torque, and efficiency of this motor are taken from a lookup table and used as a simple rotational inertial model.

Electrical power is smaller than mechanical power because the generator block is modeled such that the efficiency of output electrical power is determined by the rotational speed of the generator. In other words, there are some losses in the generator.

The lull in "zDotRel" between simulation time 270 and 280 represents a fairly regular occurrence in typical seas. The near-zero velocity causes p_j and p_k to fall below p_{min} and the rectifying valve shuts. The system response in this condition is shown in Figs. 9 and 10. Because the fluid is modeled as compressible and the closed valves have abruptly stopped the fluid flow, the fluid in the piston oscillates. This spring-like effect continues until the pressure exceeds p_{min}. This hydraulic system therefore manifests an intrinsic latching control [14].

DIRECT DRIVE PTO

Alternative to hydraulics, the direct drive power take off has less moving parts which allows a generator to capture power directly from the WEC movement. In this architecture, the PTO uses the direct buoy motion to drive the generator. The stator portion of the generator is contained in the WEC spar, while the buoy contains the magnets. This concept is illustrated in Fig. 11, and modeled using PTO-Sim in Fig. 12. The buoy movement causes the magnetic field surrounding the coils to change, the fundamental method for generating electricity. While this architecture has fewer power transformation stages and moving parts, it also has no inherent power storage capability (unlike the hydraulic system).

The direct drive approach can be constructed to deliver single or multiple-phase power by the arrangement of the generator magnets and coils. A three-phase winding was used in this model, enabling a valid comparison with the hydraulic model.

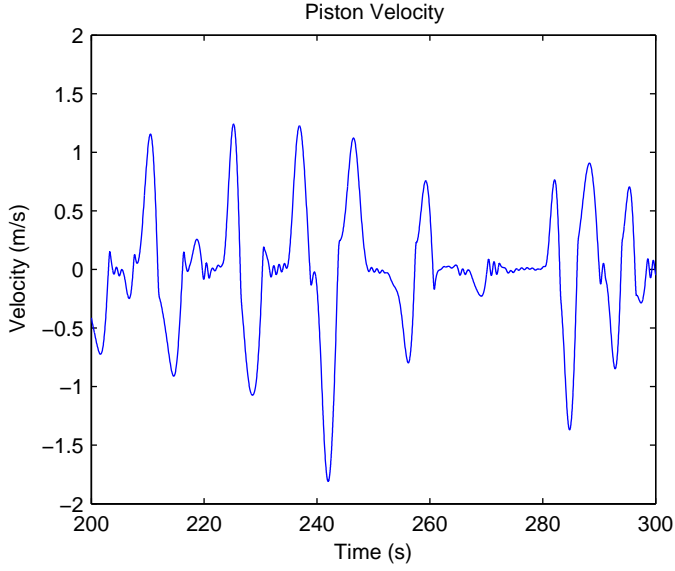The governing equation for a direct drive PTO is listed be-

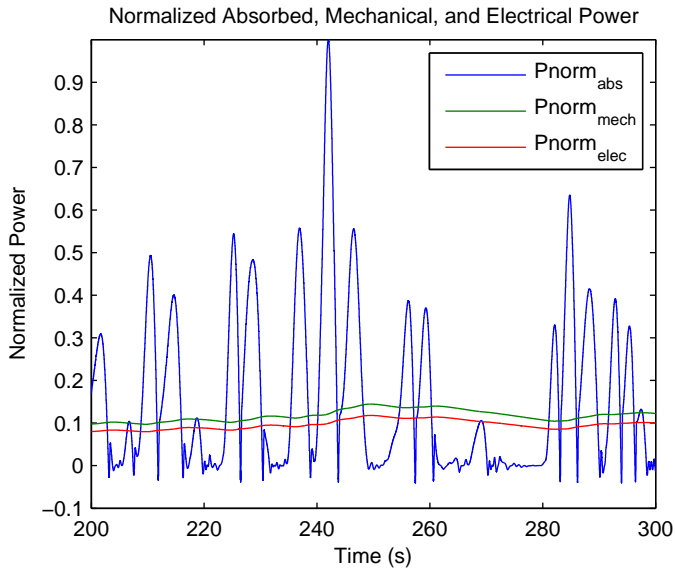**FIGURE 7**. Piston velocity for a wave of 3 meters with a dominant period of 11 seconds.

FIGURE 9. PTO force generated by the hydraulic PTO.

FIGURE 8. Absorbed, mechanical, and electrical power.
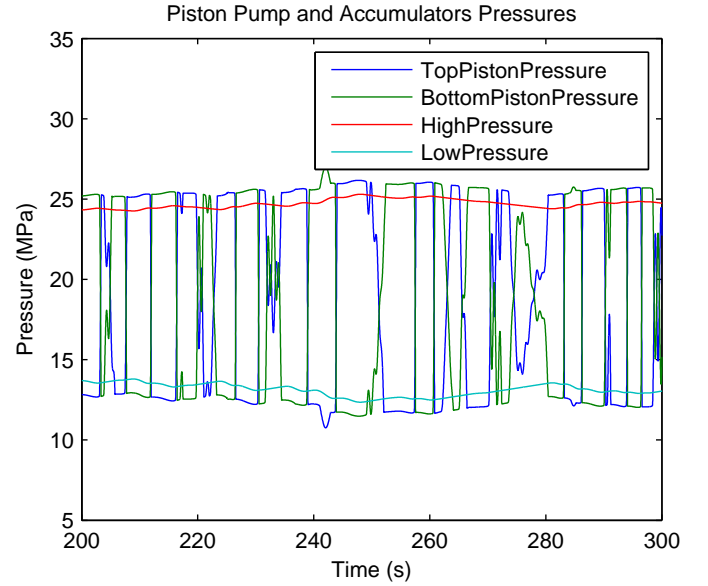

FIGURE 10. Piston pump and accumulators pressures. A check valve is open when either the top or bottom piston pressure is greater than the high pressure accumulator or less than the low pressure accumulator.

low.

$$T_{em} = k(\lambda_{sd} i_{sq} - \lambda_{sq} i_{sd}) \qquad (10)$$

where $k = P/2$ for rotational generator and $k = \pi/\tau_{pm}$ for a linear generator. P is the number of poles (P is greater or equal to 2, even number). τ_{pm} is the magnet pole pitch (the distance

measured of the magnet from the center of one pole to the center of the next pole). The generator is modeled in the synchronous reference frame, where λ_{sd} is the stator d-axis flux linkage, i_{sq} is the stator q-axis current, λ_{sq} is the stator q-axis flux linkage, and i_{sd} is the stator d-axis current. Derivation can be found in [15].

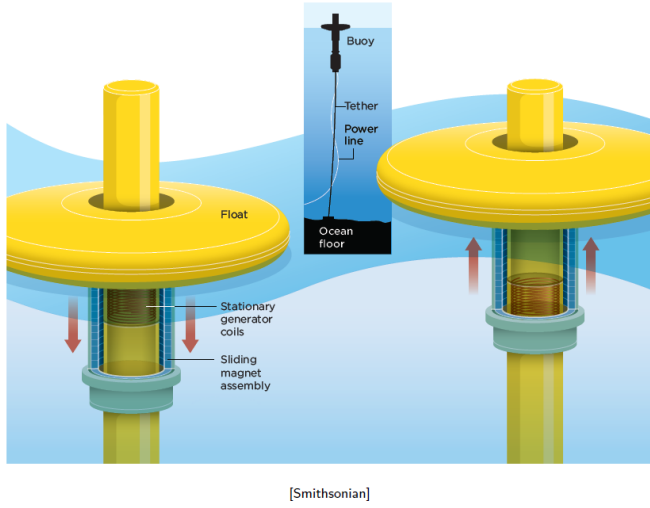Assuming the d-axis is aligned with the stator flux such that

6

FIGURE 11. Direct Drive: OSU L10. This figure shows the stationary generator coils located inside the spar and the sliding magnet assembly coupled to the float. (Image courtesy of Smithsonian Magazine) [16].
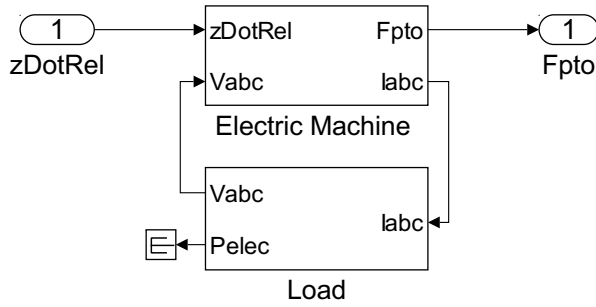

FIGURE 12. Schematic of the PTO-Sim direct drive model.

FIGURE 13. Cross section view of slots and magnets.

$\lambda_{sq} = 0$, Eq.(10) leads to Eq.(11), which describes the PTO force for a linear electric machine.

$$F_{pto} = (\pi/\tau_{pm})\lambda_{fd}i_{sq} \qquad (11)$$

The direct drive PTO model presented in this paper is based on [17]. The generator stator consists of three-phase armature windings in 4 slots per phase for a total of 12 slots. There are always 2 pole pairs in the active region at any given time as shown in Fig. 13.

The equivalent electrical circuit (Fig. 14) shows the relationship between induced voltages E_a, E_b, and E_c and the external loads R_{Load}. R_s and L_s are the winding resistance and inductance of the coil.
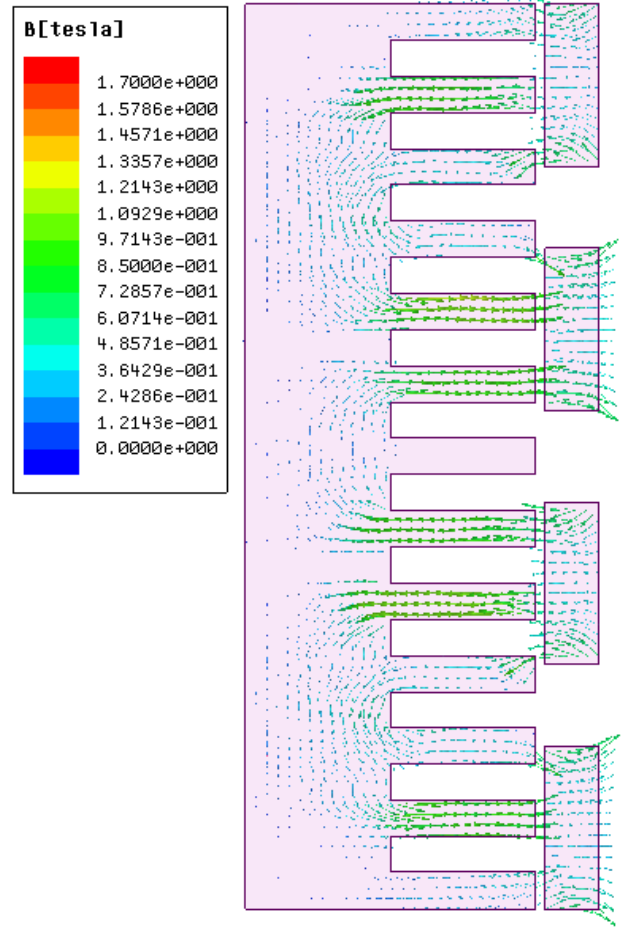
Simulations. The PTO was developed and verified with the use of regular waves. Once verified, irregular waves are applied, and the analysis can be focused on understanding the electrical power generated by the system. The same "zDotRel" is used as an input for the direct drive PTO model as was used for the hydraulic PTO, see Fig. 7.

The PTO force, derived in (11), directly follows the relative velocity because of the nature of the direct drive design (no energy storage). Figures 16 and 17 show voltage and current in the external load. It should be noted that the magnitude of the voltage and current depends on the wave climate, and the WEC design parameters [17]. The absorbed and electric power are shown in Fig. 18.
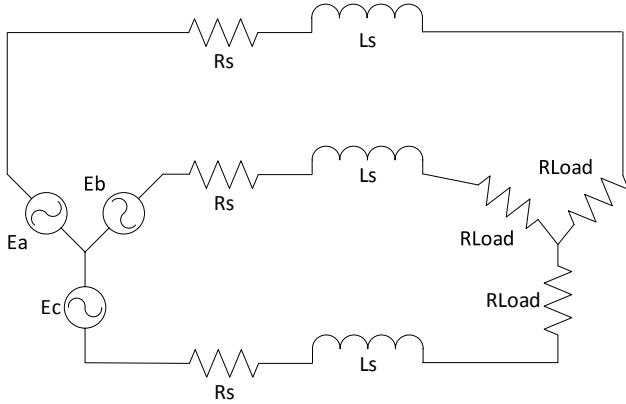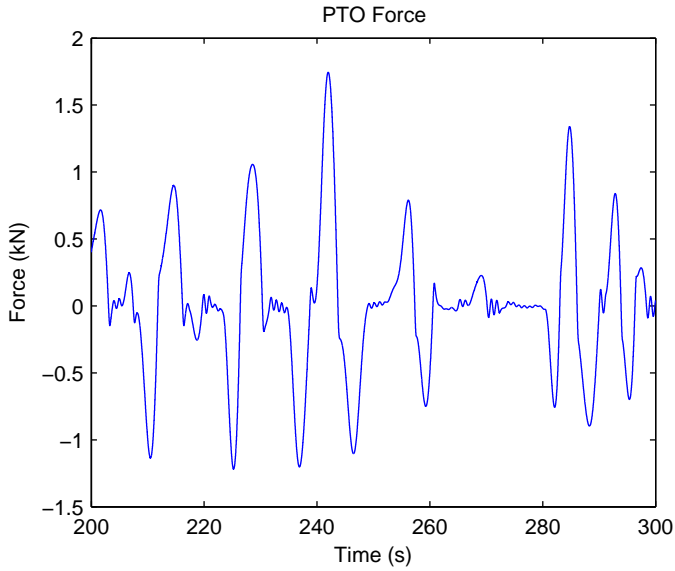
FIGURE 14. Back EMF circuit.

FIGURE 15. Direct drive PTO force.

FIGURE 16. Direct drive 3-phase line to neutral load voltage. As the PTO speed increases, both voltage magnitude and electric frequency increase.

FIGURE 17. Direct drive 3-phase current.

Generated Power Comparisons

The usefulness of the PTO-Sim tool is exemplified by comparing the results from the two different architectures. The output electrical power for each PTO architecture is normalized and plotted in Fig. 19. This figure clearly shows the native storage capability of the hydraulic system, which manifests as a smoother power profile. In contrast, the direct drive architecture power output is a direct reflection of the incident sea state.

Although Fig. 19 shows a comparison between the two PTOs, it is hard to determine which PTO system yields more power because in order to do so, the direct drive system would need to have a storage. The purpose of this comparison is to show that each PTO has its pros and cons.

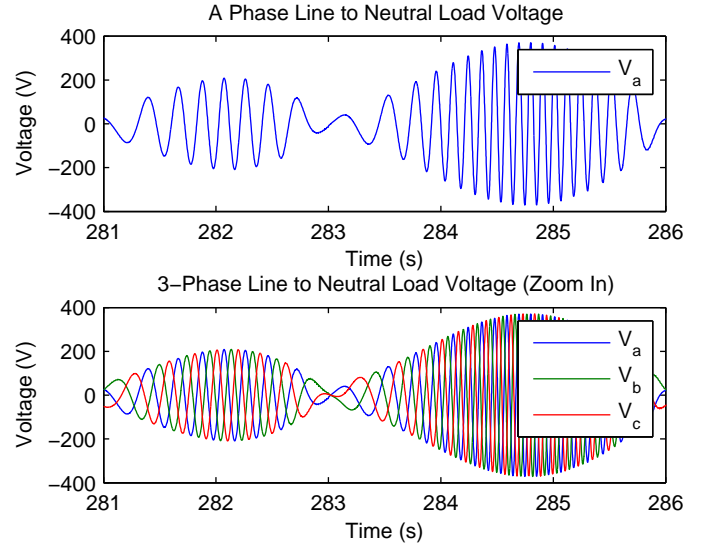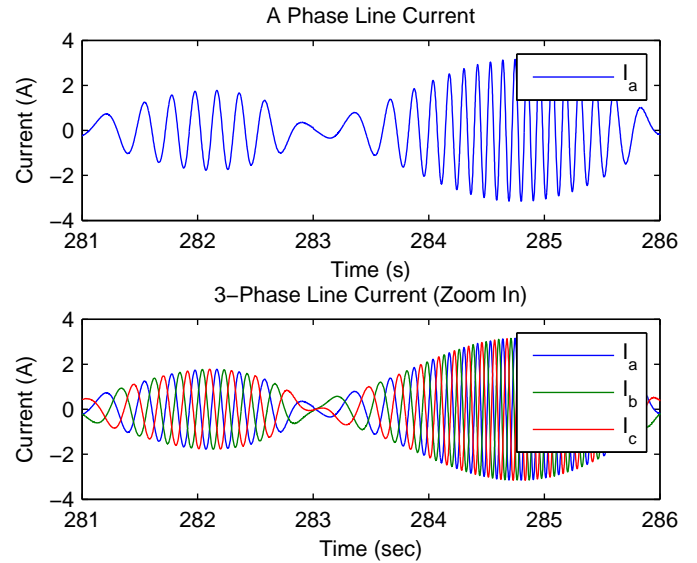Current WEC-Sim allows the user to get an idea of what the power production will be; with little knowledge of drive-trains/power electronics, etc. However, if the user wants to design a PCC and compare the benefits of different PCC options, that is where PTO-Sim will come to play. It should be noted that, this obviously requires the user to be more knowledgeable and careful when designing the PTO model. Therefore, the goal of designing PTO-Sim is to abstract the end-user from the details
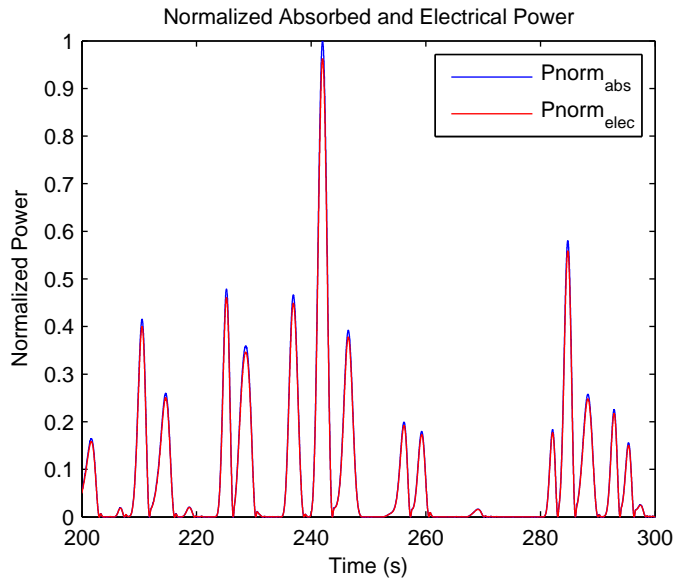
8

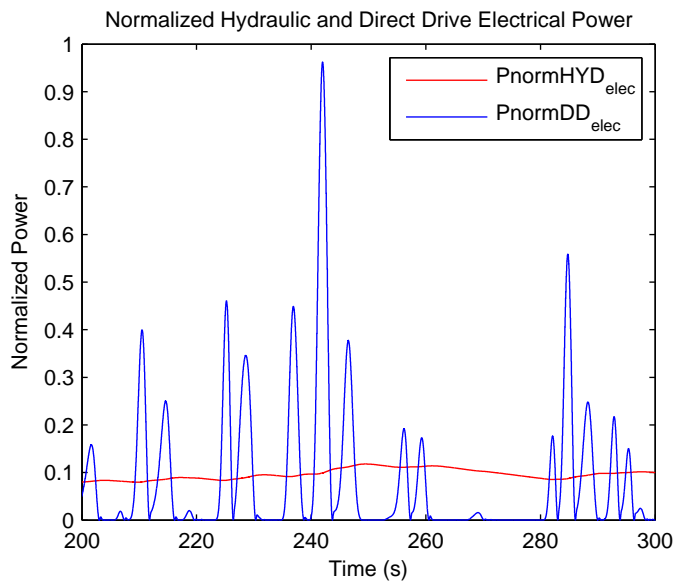**FIGURE 18**. Absorbed and Electrical Power. Efficiency is calculated to be about 96 %.

FIGURE 19. Comparison Between Normalized Hydraulic and Direct Drive Electrical Power.

but to make the the wave energy converter more accessible.

CONCLUSION

This paper illustrates the development and application of PTO-Sim, the WEC-Sim module responsible for accurately modeling the WEC's conversion of mechanical power to electrical power through its PTO system (or power conversion chain, PCC). While the initial release of WEC-Sim, Version 1.0, included the ability to model a WEC's PTO system as a simple linear damper, PTO-Sim allows users to model more complicated WEC PCCs. To show the functionality of PTO-Sim, two applications of PTO-Sim were given in the paper. One of a hydraulic PTO system, and one of a direct drive PTO system. These two configurations were chosen because they reflect the two most common WEC PTO systems for WECs with TRL 5+. The simulation results included illustrate the typical high-efficiencies of direct drive systems, but also illustrate the power smoothing (i.e., energy storage) inherent to hydraulic systems.

The current release of the WEC-Sim code, v1.0, includes linear damping to model WEC PTOs. Future work on PTO-Sim includes development of fully two-way coupled WEC-Sim and PTO-Sim models for both the hydraulic and direct drive PTOs. The hydraulic and direct drive PTO-Sim libraries will be included in future releases of the WEC-Sim code. Also included in the future WEC-Sim releases will be example applications of the PTO-Sim library to model hydraulic and direct drive PTO systems based on the work presented in this paper.

REFERENCES

[1] "Wec-sim version 1.0."

[2] Y. Yu, Ye Li, Kathleen Hallett, and Chad Hotimsky, "Design and analysis for a floating oscillating surge wave energy converter," in *Proceedings of OMAE 2014*, (San Francisco, CA), 2014.

[3] MJ Lawson, Y. Yu, Adam Nelessen, Kelley Ruehl, and Carlos Michelen, "Implementing nonlinear buoyancy and excitation forces in the WEC-sim wave energy converter modeling tool," in *Proceedings of OMAE 2014*, (San Francisco, CA), 2014.

[4] Kelley Ruehl, Carlos Michelen, Samuel Kanner, Michael Lawson, and Y. Yu, "Preliminary verification and validation

of WEC-sim, an open-source wave energy converter design tool," in *Proceedings of OMAE 2014*, (San Francisco, CA), 2014.

[5] Y. Yu, Michael Lawson, Kelley Ruehl, and Carlos Michelen, "Development and demonstration of the WEC-sim wave energy converter simulation tool," in *Proceedings of the 2nd Marine Energy Technology Symposium*, (Seattle, WA, USA), 2014.

[6] Y. Kamizuru, *Development of Hydrostatic Drive Trains for Wave Energy Converters*. PhD thesis, RWTH Aachen University, Germany, 2014.

[7] M. Reed, R. Bagbey, A. Moreno, T. Ramsey, and J. Rieks, "Accelerating the us marine and hydrokinetic technology development through the application of technology readiness levels (TRLs)," in *Proceedings of Energy Ocean*, 2010.

[8] K. Ruehl and D. Bull, "Wave energy development roadmap: design to commercialization," in *Oceans*, pp. 1–10, IEEE, 2012.

[9] D. N. Veritas, "Recommended practice dnv-rp-a203– qualification procedures for new technology," 2001.

[10] "WHTP marine hydrokinetic technologies database: Project profile."

[11] "Sandia national laboratories: Reference model project (rmp)."

[12] S. Casey, "Modeling, simulation, and analysis of two hydraulic power take-off systems for wave energy conversion," Master's thesis, Oregon State University, Corvallis, OR, 2013.

[13] H. E. Merritt, *Hydraulic control systems*. John Wiley, 1967.

[14] J. Falnes, *Ocean waves and oscillating systems*. Cambridge University Press, 2005.

[15] N. Mohan, "Advanced electric drives," *Minneapolis: MN-PERE*, 2001.

[16] E. Rusch, "Catching a wave, powering an electrical grid," *Smithsonian Magazine*, July 2009.

[17] J. Prudell, M. Stoddard, T. Brekken, and A. von Jouanne, "A novel permanent magnet tubular linear generator for ocean wave energy," in *Energy Conversion Congress and Exposition, 2009. ECCE 2009. IEEE*, pp. 3641–3646, IEEE, 2009.